Use of 5G and mmWave radar for positioning, sensing, and line-of-sight detection in airport areas

Fathia Ben Slama*, Kanaan Abdo*, Eliot Vignaud*, Alexandre Simonin*,
Elena Simona Lohan†, Hadeel S. Obaid†, Taylan Yesilyurt†, P. A. D. Nirmal Jayawardana †, Bo Tan†,
Christophe Morlaas‡, Alexandre Duchevet‡, Mohamed Ellejmi§
*ALTYS Technologies, Toulouse, France;
†Faculty of Information Technology and Communication Sciences, Tampere University, Finland;
‡ENAC, Toulouse, France; §EUROCONTROL, Brétigny Sur Orge, France
{fathia.benslama, kanaan.abdo, eliot.vignaud, alexandre.simonin}@altys-tech.net,
{elena-simona.lohan, hadeel.obaid, taylan.yesilyurt, nirmal.jayawardana, bo.tan}@tuni.fi,
{christophe.morlaas, alexandre.duchevet}@enac.fr, mohamed.ellejmi@eurocontrol.int

***Abstract*—This paper explores innovative low-cost technologies, widely used outside of Air Traffic Management (ATM), for use in airport surface surveillance. These technologies consist of a 5G-signal-based surveillance solution and a millimeter wave (mmWave) radar augmented with artificial intelligence (AI). The 5G solution is based on the combination of 3D Vector Antenna, innovative signal processing techniques, and hybridization techniques based on time-of-arrival and angle-of-arrival estimates with uplink and downlink 5G signals, as well as Machine Learning (ML)-based Line of Sight (LOS) detection algorithms. The mmWave solution is based on mmWave radar for non-cooperative target's positioning and sensing, combined with deep learning for objects classification. Standalone 5G positioning accuracy reaches m-level accuracy in LOS scenarios and it is better with downlink reference signals than with uplink ones, while it deteriorates quite drastically in NLOS scenarios. LOS detection accuracies above 84% average accuracy can be achieved with ML. The mmWave radar is tested in different scenarios (short, medium and long range) and it provides cost-effective surface surveillance up to few hundred meters (depending on the object radar cross section RCS) with ±60° field of view. The work is being conducted within the H2020 European-funded project NewSense and it delves into the 5G, Vector Antennas, mmWave, and ML/AI capabilities for future ATM solutions.**

***Keywords*—5G, Angle of Arrival (AoA), Air Traffic Management (ATM), Artificial Intelligence (AI), Communications, Line of Sight (LOS) detection, Machine Learning (ML), Millimetre Wave, Positioning, Sensing, Surveillance, Time of Arrival (ToA), Vector Antenna (VA), Synthetic-aperture Radar**

I. Introduction and motivation

The increasing growth in air traffic is putting pressure on airports for greater capacity and increased safety, which is pushing airports to be equipped with an advanced surface movement guidance and control system (A-SMGCS). While most of the world's largest airports have initiated the implementation of an A-SMGCS, small and medium-sized airports cannot afford such systems due to the high costs of the necessary infrastructure (multilateration deployment (MLAT) and surface movement radar (SMR)). Alternative low-cost solutions for airport surface surveillance such as cameras and LIDAR (Laser Imaging Detection And Ranging) have been assessed in SESAR 2020 Exploratory Research ENVISION project and SESAR 2020 Industrial Research project EARTH (solution PJ02.06) and results demonstrated that the optical sensors have limited performances in low visibility conditions that could be caused by rain, frog, snow, darkness, dazzling sunlight, and other meteorological constraints.

The potential of radio frequency (RF) signals and Single/Multiple Input Multiple Output (SIMO/MIMO) systems in measuring an object's position and velocity seamlessly and independently of visibility conditions have proved their efficiency in automotive and industrial applications [1] [2] [3] [4] [5]. In one hand 5G networks, already in commercial phase and expected to be large-scale deployed in the next decades - thus offering the opportunity to use 5G network infrastructure -, in the other hand the increasing use of mmwave radar for automotive and industrial applications, and the recent interest in applying deep learning algorithms to radar data should be considered when looking for alternative affordable surveillance solutions for the future ATM. Thus, the NewSense project proposes innovative surveillance solutions to improve airport surface surveillance and situational awareness in all weather and visibility conditions. These positioning and sensing solutions, completely new for ATM context, are based on timing and angle measurements from 5G RF signals, mmWave radar augmented with artificial intelligence (AI), and 5G RF-based radar as illustrated in Fig. 1. The novel work done in the scope of this research includes:

- The design of a 5G-signal-based surveillance solution for the airport surface including a 3D vector antenna (3D VA), a 5G positioning function to measure cooperative targets position using their transmitted 5G RF signals, and a ML-based LOS detection mechanism
- The design of a radar-like system relying on 5G signals to calculate non-cooperative targets position from reflected 5G base station RF signals.
- The evaluation of a low-cost mmWave radar as a non-cooperative surveillance solution to position and classify targets using reflected mmWave radar signals and deep learning methods.

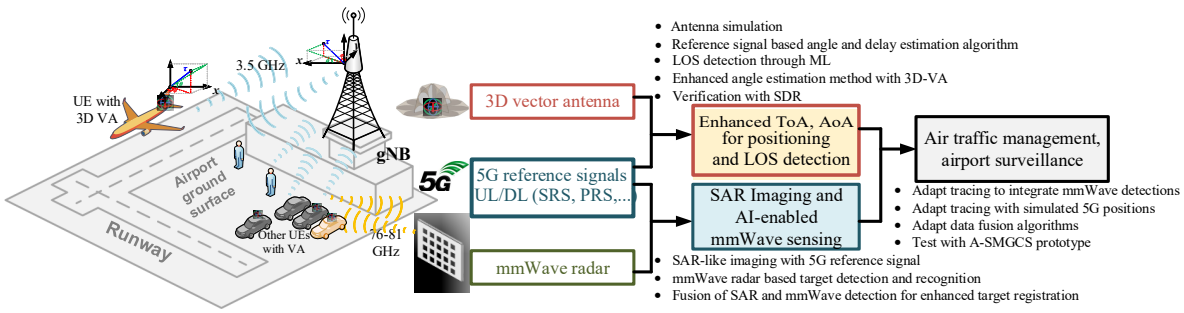

Figure 1. Illustration of the integrated-concept architecture for airport surveillance

- The validation through in-lab measurements of some of the proposed solution. Part of our measuremet data has also been made available in open-access on Zenodo repository [6].

This paper is elaborated in continuity of the previous work detailed in [7], in which we described in the 5G framework the working principle of the 3D-VA, the 5G reference signals, the angle-delay estimation algorithms, and the imaging algorithms. In the mmWave radar framework, we described FMCW mmWave radar working principle and the signal processing chain applied to mmWave signals. We provided also the preliminary results for both frameworks.

In this paper, we will describe the implemented channels models with 5G signal and the obtained results in Section II. The simulations with 3D-VA are provided in Section III. In Section IV, mmWave radar setup, mmWave measurements scenarios, ML algorithms and obtained results are described. In section V LOS detection with 5G signals is explained.The measurement setup using 5G signals and the 3D-VA, and the corresponding results are provided in Section VI At last, the conclusion and future work are given in the Section VII.

II. Simulation Toolboxes for 5G Signals

The main idea of 5G-signal-based positioning algorithms is exploiting the always-on reference signals of 5G NR to estimate the position of user equipment (UE). Our previous work in [7] has introduced the 5G reference signals used in positioning and the time-based and angle-based estimators. We have now developed an in-house Matlab-based simulator for uplink and downlink 5G signals that is based on Matlab 5G toolbox and covering three types of positioning-related reference signals, namely Sounding Reference Signals (SRS) for uplink (UL) and Positioning Reference Signals (PRS) and Channel State Information Reference Signals (CSI-RS) for downlink (DL). Our simulator also comprises four types of channel models: the Additive White Gaussian Channel (AWGN) model taken as benchmark, the 3GPP Tapped Delay Line (TDL) and Cluster Delay Line (CDL) models, and the Matlab WINNER II channel model. AoA-based and ToA-based estimators for the three types of reference signals and a selected NLOS channel (CDL-A channel) are shown in Fig. 2. Similar behaviour was observed for LOS channels. Clearly, time-based estimates are much more sensitive to the type of the reference signal than angle-based estimates, with PRS providing the best performance and CSI-RS providing the worst performance. AoA-based estimates are also much more accurate than our ToA-based estimates, no doubt due to the fact that a high-resolution MUSIC algorithm was used for AoA, while a simple correlation-based estimator was used for ToA results.

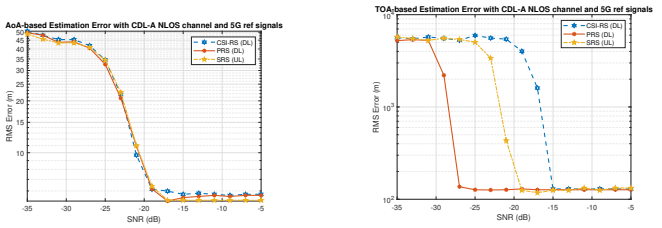

Figure 2. Root Mean Square positioning Errors (RMSE) for CSI-RS, SRS, and PRS signals in a a CDL NLOS channel. Left: AoA estimator; right: ToA estimator.

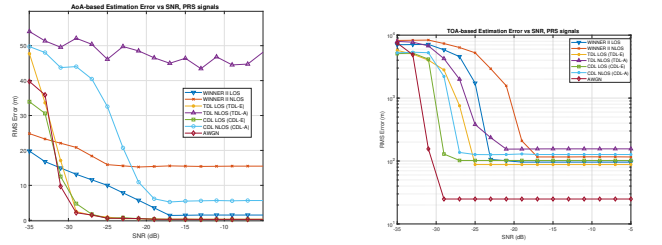

Figure 3. Root Mean Square positioning Errors (RMSE) for different channel types, based on PRS signals. Left: AoA estimator; right: ToA estimator.

Fig. 3 also shows the positioning error performance under five channel types: AWGN, two LOS channels (TDL and CDL), and two NLOS channels (TDL and CDL). The left-hand plots are based on AoA estimators and the right-hand plots on ToA estimator. Clearly, the performance in AWGN and LOS channels is significantly better than in NLOS channels. The saturation point in AWGN channels and ToA-based estimation is due to the sampling frequency that defines the maximum resolution in time domain; we used a sampling frequency of 15.36 MHz, which limits the time-domain resolution to 19.5 m. Higher time resolutions can be achieved with higher sampling frequency, at the expense of a higher complexity and longer simulation times. WINNER II channels are the most challenging for a ToA-based estimator, followed by TDL channels, while TDL channels are the most challenging for AoA estimators, followed by CDL channels. AoA-based

estimators also have better results than ToA-based estimators for all the considered wireless channels.

III. Simulations with 3D Vector Antenna

A. Vector antenna description

The 3D-VA is constituted from an arrangement of Vivaldi antennas. it is particularly interesting for this application since it exhibits a directional radiation pattern with a stable gain over a wide bandwidth and beamwidth. In addition to that, it presents a good polarization discrimination allowing DoA capability with physical characteristics of low-profile, light-weight, and low-cost.

The proposed 8-port vector antenna is here supposed to retrieve independently the six components (E_x, E_y, E_z, H_x, H_y, H_z) of an incoming EM wave in the entire 3-D space. The corresponding sets of weighting coefficients and EM components are reported in Table I. The corresponding set of six radiation patterns will be called RPC0. In addition to that, additional set of radiation patterns (RPCs) can be used in order to improve the DoA performances. The additional weighting coefficient used to define these additional RPC's are obtained from a parametric analysis [8]. We will focus particularly in two RPCs called RPC1 and RPC2 that consists of a set of different weighting coefficients that provide same radiation patterns with a rotation of 90^o along the azimuth angle ϕ. The RPC1 is chosen to improve the vertical polarized DoA while the RPC2 to improve the horizontal polarized DOA. Only port 1 to 4 are used for RPC1 while Port 5 to 8 are used for RPC2.

TABLE I. Set of weighting coefficients assigned to the signals received at the eight antenna ports for synthesize the six main radiation patterns and additional RPCs

RPC	Port 1	Port 2	Port 3	Port 4	Port 5	Port 6	Port 7	Port 8
0	0	0	0	0	1	1	-1	-1
	0	0	0	0	1	-1	-1	1
	1	1	1	1	0	0	0	0
	0	-1	0	1	0	0	0	0
	1	0	-1	0	0	0	0	0
	0	0	0	0	1	-1	1	-1
1	1	1	1	-1	0	0	0	0
	1	1	-1	1	0	0	0	0
	1	-1	1	1	0	0	0	0
	-1	1	1	1	0	0	0	0
2	0	0	0	0	1	1	1	-1
	0	0	0	0	1	1	-1	1
	0	0	0	0	1	-1	1	1
	0	0	0	0	-1	1	1	1

B. Simulation experiments

In this section, the DoA arrival accuracy is assessed at 3.5 GHz according to the RPCs used. The AoA estimation accuracy refers to the angular error between the estimated and expected angles of an incoming EM wave. The AoA accuracy depends on the signal to noise ratio which is defined in the MUSIC algorithm and the propagation effects of the corresponding EM wave. This parameter is usually given by Root-Mean-Square (RMS) values. More specifically, the AoA angular accuracy may be defined with

$$\epsilon_{RMS}(\Omega) = \sqrt{\frac{1}{L}\sum_{i=1}^{L}|\Omega - \hat{\Omega}|^2} \quad (1)$$

where Ω is the expected angle (along the azimuth ϕ or elevation angle θ), $\hat{\Omega}$ is the estimated angle, and L is the number of trials.

On the other hand, the angular distance Δ_α can be defined as the minimal distance between the expected angle set (θ, ϕ) and estimated direction ($\hat{\theta}$, $\hat{\phi}$) given by

$$\Delta_{\alpha_{RMS}} = \sqrt{\frac{1}{L}\sum_{i=1}^{L}|\Delta_\alpha(\theta,\ \phi)|^2} \quad (2)$$

with,

$$\Delta_{\alpha_{(\theta,\ \phi)}} = \cos^{-1}(\cos\theta\cos\hat{\theta} + \sin\theta\sin\hat{\theta}\cos(\phi - \hat{\phi})) \quad (3)$$

Table II shows the conditions applied for the scenario under test in order to compute the angular distance associated with the θ, and ϕ angles of the proposed VA.

TABLE II. Parameters used for angular distance estimation

Number of incoming EM fields	1
Polarization of the incoming EM field	Vertical
Angular coverage	$\phi \in [0^\circ\ ;\ 360^\circ]$ $\theta \in [0^\circ\ ;\ 120^\circ]$
Angular resolution	$\Delta\phi = 5^\circ$ $\Delta\theta = 5^\circ$
Incoming EM field power density	-91 dBW.m^{-2}
Noise power level	-111 dBm
Mean SNR	9 dB
Number of DoA estimation	20
Snapshots per DoA estimation	50
Frequencies of interest	3.5 GHz

The figure 4 depicts the simulated angular distance RMS error for θ, and ϕ and the angular distance ($\Delta_{\alpha_{RMS}}$) using the MUSIC algorithm for an azimuth angular range of 360° and an elevation angular range of 120° i.e. -30° toward the bottom direction. As a recall the 0° elevation angle is toward the zenith. The six components derived from the proposed VA (RPC0) are considered only. The maximal error is around 1.5° for elevation angle in a range of 80° to 1000° and around 30°. The $\Delta_{\alpha_{RMS}}$ error is due to a mixed error on the ϕ and θ angle error.

In figure 5 the six components derived from the proposed VA (RPC0) and the additional RPC's 1 and 2 are considered. The error for both angles is reduced. The VA is now capable to accurately estimate sources in the bottom half-space until

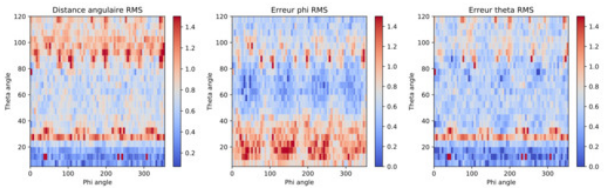

Figure 4. Angular distance, θ, and ϕ error for $SNR = 9$ dB and with RPC0 used.

$-30°$. A small error persist around $30°$ and $100°$ for elevation angle.

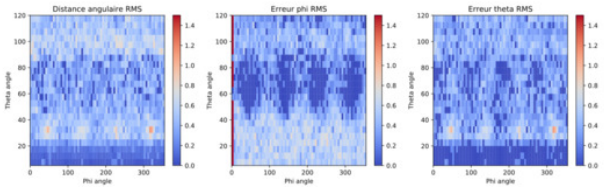

Figure 5. Angular distance, θ, and ϕ error for $SNR = 9$ dB and with RPC0, RPC1, and RPC2 used.

IV. mmWave radar augmented with AI

In addition to the assessment of a 5G-signal based positioning solution, the objective in this study is to localize non-cooperative targets on the airport surface and identify their type (mainly aircraft, vehicle and person) using Frequency Modulated Continuous Wave (FMCW) mmWave radar and AI. Understanding the technology concept of this type of radar is essential to properly configure the mmWave sensor and optimize its use. The mmWave technology description, the operational principles of an FMCW mmWave radar and the data processing chain to detect and calculate the target's range, angle and velocity have been detailed in [7].

A. mmWave radar configuration

Three scenarios have been used to configure the radar and the parameters have been computed in order to have the best precision depending on the targeted area. On the airport surface, we distinguish three areas that should be covered by the radar: the parking, the taxiway and the runway. The first scenario is the Long-Range Radar (LRR) that will cover a section of the runway. The second scenario is the Medium Range-Radar (MRR) that will cover the taxiway and the parking area. Finally, the Short Range-Radar will cover mainly the parking area. Configuration parameters and corresponding range and velocity values are given in Table III.

B. Testbed description

The radar testbed is composed of the mmWave radar AWR2243BOOST EVM [9] combined with the data capture module DCA1000EVM [10] mounted on a tripod. A host computer is used to record received data from the DCA1000EVM for post processing purposes. A camera is also used in order to keep the ground truth image corresponding to radar data.

TABLE III. AWR2243 [9] configuration for LRR, MRR and SRR scenarios

Parameter	LRR	MRR	SRR
Idle time/Inter-chirp duration (µs)	2.5	3	3
Number of ADC samples	128	256	256
ADC sampling frequency (Msps)	22.50	14.40	7.00
Chirp duration active/Ramp end time (µs)	9	21	40
Number of chirps per profile	255	128	128
Frequency slope (MHz/µs)	10.042	14.001	15.015
Number of RX channels	4	4	4
Number of TX channels	2	2	2
Frequency Limit Low (GHz)	79.50	79.50	79.50
Maximum theorical range (m)	302.27	138.75	62.89
Range resolution (m)	2.624	0.602	0.273
Maximum velocity (Km/h)	147.51	70.60	39.33
Velocity resolution (m/s)	0.321	0.306	0.171

Finally, we use a portable battery to power the devices as most of the testing is done outdoors.

C. Positioning results

Several measurements with the radar have been conducted in laboratory, underground and external parkings with persons and vehicles, and in real air-side environment (Muret–Lherm Aerodrome, France). Measurements done in external parking and in airfield are very interesting for the study as they make possible to assess the sensor in an environment very close to the targeted deployment environment. Measurements for SRR, MRR and LRR scenarios have been conducted in an external parking for moving person and vehicle. These scenarios have been also tested at Muret airfield for persons in the parking area and for General Aviation (GA) aircraft in the parking, taxiway, and a segment of the runway.

The radar is able to detect a person to up to 66 meters, a vehicle to up to 113 meters and a GA aircraft to up to 83 meters. A truck has also been detected at a distance of 138 meters. Some measurements results are shown in Fig.6. Within the same configuration (transmit power, SNR, RX and TX antenna gain) and as commercial aircraft have an higher Radar Cross Section (RCS) than targets used within this study, we could estimate that the radar may detect commercial aircraft up to few hundred meters. The maximum range of the radar could be increased if the radar transmit power increases. As examples, the maximum transmit power of an ATC primary surveillance radar (PSR) is 100 kWatt [11] and typical Surface Movement Radar has a transmitting power superior than 180 Watt. In the scope of this study we used an evaluation module for the mmWave radar with a transmit power up to 0.016 Watt.

The range resolution obtained by the mmWave radar makes possible to distinguish two close objects. Fig.6 shows a moving person detected near the aircraft and the radar was capable to distinguish it from the aircraft at a distance less than 1 meter.

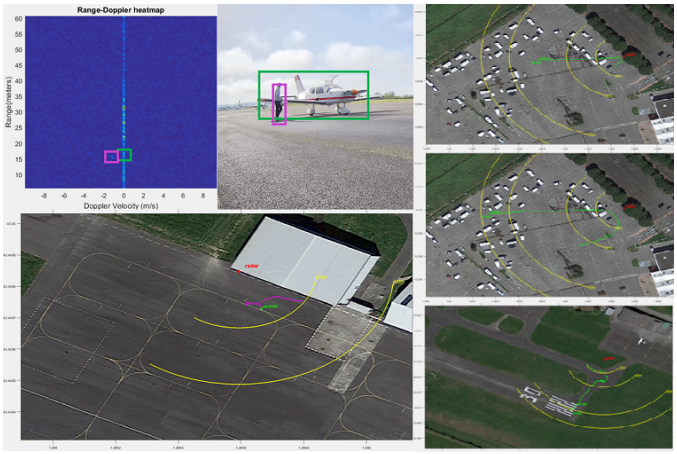

Figure 6. mmWave radar positioning results, no tracking filter is applied

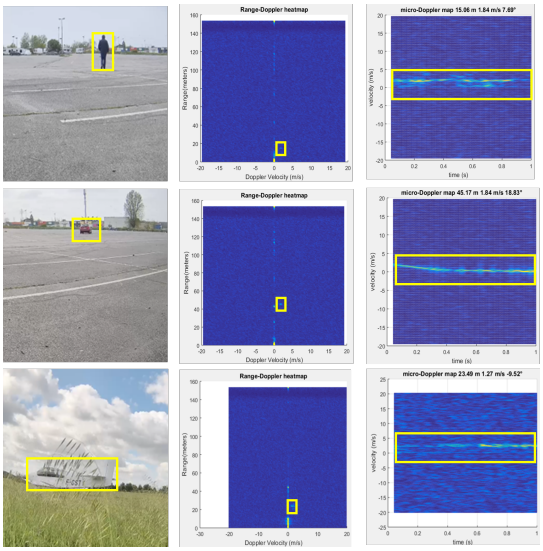

Figure 7. Camera image, Range-Velocity heatmap and STFT heatmap of person, a car, and GA aircraft

D. AI applied to mmWave signals

ML will be used to process mmWave radar signals for detection and classification purposes. As there are not many open-access datasets on mmWave radar data, and even non-existent in the airport context, a dataset should be created by making several measurements and tests in different environment (external parking, roads, etc.) and especially at the airport.

1) Classification using the Micro-Doppler Signature: A Micro-Doppler Signature of a target results from the additional motions of the target (rotation, vibration, etc.), other than main mass translation, which generates a time varying frequency modulation imparted in the echo. This signature contains target's features and therefore can be used for classification. The Micro-Doppler is calculated using the Short-Time Fourier Transform (STFT) of the signal during a short laps of time (in our case, 1 second).

Fig.7 shows examples of STFT heatmaps (in the third column). STFT heatmaps contain information about how the object is moving as a whole, and how individual part within the object are moving. For example, with a propeller plane, the STFT heatmap will display both the Doppler shift of the moving plane, as well as the Micro-Doppler shifts of the propeller. For a moving person, it shows his velocity and also the Micro-Doppler of his arms and legs.

We chose EfficientNetV2 [12] as the model for the classification for 3 main reasons:

- At the time of the model selection, EfficientNetV2 was amongst the best neural network on several image classification benchmarks.
- As discussed earlier, our dataset will be smaller than images dataset. Moreover, each sample is longer to process, since the dimension of the last channel is greater than the traditional 3 for Red Green Blue images. EfficientNetV2 was designed to have less weights (thus needing less data) and shorter training time than other state-of-the-art models.
- EfficientNetV2 is widely used, which makes it accessible with pre-trained weights in several libraries.

The dataset includes 2802 examples, with 2324 examples of aircrafts, 240 examples of pedestrians and 238 examples of cars. As such, the classes present in the dataset are imbalanced. This means that accuracy alone cannot be used to evaluate different models, because a model that always answer "aircraft" would have an accuracy of 83% in our case, while giving nothing of value. To ensure that our model does not act that way, we train it with a weighted loss function. This means that misclassifications during training are penalized more the less a class is present in the dataset. We trained several models while varying the degree to which the minority classes were favorized, and even in the most favorable case, planes were detected correctly with an accuracy of 93,6%, vehicle with an accuracy of 61,5% and pedestrian with an accuracy of 34,0%.

We see two solutions as the most promising to improve the model further. The first one simply consists of gathering more data, especially for vehicles and pedestrians. The second is to use data augmentation, to create new examples from our current ones. It could be done at two levels: at the STFT heatmaps level or directly at the raw radar data level. Radar data augmentation is a less studied field than image data augmentation, but new research tries to tackle this issue [13]. In order to ameliorate classification results with Micro-Doppler data, future work will consist of creating new STFT heatmaps from our current radar data by simply shifting the time window used to generate the heatmaps.

2) Classification using the Range-Angle heatmap: The previous method was showing a lot of promise, but the reliance on the Doppler effect made it unusable when a target was not moving at all. For that reason, we tried an alternate method, based on the Range-Angle heatmap. The proposed method would use image detection (i.e., means classification and localization of the object of interest in the image) instead of image classification. The image detection method used is YOLOv4 [14]. Like EfficientNetV2, YOLOv4 was chosen

for his performance on image detection benchmark and for his wide use in the industry. At the beginning, we tried to train the model using the Range-Angle heatmap obtained using the 3FFT [7]. However, the high-level of noise and the low resolution in these heatmaps make it hard to create the image that YOLO would be used on. We have tried then another direction-of-arrival estimation method: the high-resolution MUSIC algorithm. Thus, we have obtained better results for the Range-Angle heatmaps as illustrated in Fig.8. Future work will be to train the model and evalutate the performance of this model in objects' detection.

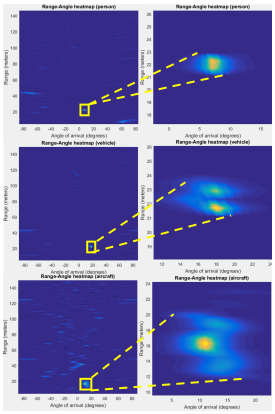

Figure 8. Examples of Range-Angle images on the left and zoom on targeted object on the right

V. LOS DETECTION

The accuracy of positioning is highly deteriorating in the presence of NLOS, therefore the classification into LOS and NLOS scenarios is a fundamental block towards a comprehensive 5G-based positioning solution. There are typically two main classes of LOS detection algorithm: one based on signal processing models, where different characteristics of the received signal are extracted from measurement data and compared to a threshold, and another one based on ML, and relying on some training phase, where relevant features are extracted from the available data and then ML algorithms are applied to classify the data based on those features. Examples from the first category are: kurtosis-based detection [15], [16], cross-polarization discrimination [17], channel impulse response entropy [18], Rician-factor-based detection [16] or time-space-frequency correlation [19]. Examples from the second, ML-based, category for LOS detection can be found in [20]–[24]. ML-based algorithms are typically understood to exhibit better performance than the model-based algorithms and they have been poorly studied so far in the context of 5G signals. Therefore, our focus has been on ML-based LOS-detection, by using our in-house 5G signal simulator (Matlab-based) and two classes of wireless channels: Tapped Delay Lines (TDL) and Clustered Delay Lines (CDL) channel models. Each class had five sub-categories (denoted A to E), with categories A-C modeling NLOS cases and categories D-E modeling LOS cases. More details about TDL and CDL channels can be found, for example, in [25] and they are widely known in the 5G research community. In our analysis, 1000 random samples were generated per channel category (total 5000 samples); 80% of data was used for training and 20% of data for testing. We studied both downlink and uplink configurations, but since the obtained results were similar, for clarity purpose we only show here the downlink results based on PRS reference signals. An example of channel impulse response (CIR) obtained from the correlations with PRS downlink signals under LOS and NLOS scenarios is shown in Fig. 9 for CDL channels.

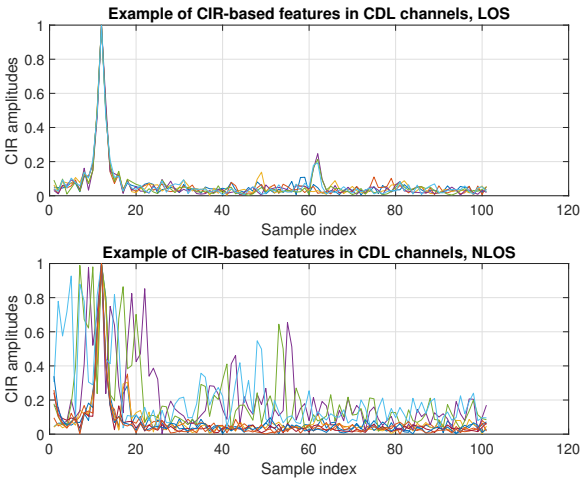

Figure 9. Examples of correlation outputs under LOS and NLOS scenarios with CDL channels (different curves show different realizations of the channel). SNR= 0 dB; PRS downlink signal.

Based on the literature search, several features were investigated for use with ML, namely time-domain correlation, frequency-domain spectrum, and kurtosis of the received signal. Results comparing the LOS detection probability under different features are shown in Table IV with CDL and TDL channels and with Support Vector Machine (SVM) classifier with medium Gaussian kernel.

TABLE IV. LOS DETECTION PROBABILITIES WITH SVM CLASSIFIER AND DIFFERENT NUMBER OF FEATURES

Features	TDL	CDL
1 feature (time)	84%	90%
1 feature (frequency)	77%	85%
1 feature (kurtosis)	69%	71%
2 features (time + frequency)	83%	88%
2 features (time + kurtosis)	78%	86%
2 features (frequency+kurtosis)	83%	86%
3 features (time + frequency + kurtosis)	84%	88%

The results in Table IV show that time-domain features are the strongest among the other investigated features and combining several features together cannot surpass the performance with a single feature only when time-domain correlation is used as the single feature. In addition, LOS detection

Figure 10. The hardware configuration schematic.

probabilities were slightly better for CDL channels than for TDL channels, no doubt due to the higher richness of time-domain features in a CDL compared to TDL. Different ML classifiers have also been investigated and an example of results is shown in Table V for five selected classifiers and time-domain features. As the selected classifiers are well-known from the ML literature, their exact description is not added here for lack of space.

TABLE V. LOS DETECTION PROBABILITIES WITH SVM CLASSIFIER AND DIFFERENT NUMBER OF FEATURES

Classifiers	**TDL**	**CDL**
SVM, medium Gaussian	84%	90%
XGboost	80%	89%
Random Forest	79%	87%
Neural Networks (NN)	81%	85%
Cosine Nearest Neighbours	79%	85%

The SVM classifier gave the best results, followed by XGboost and NN classifiers. Again, the results based on CDL channels were slightly better than with TDL channel.

VI. MEASUREMENTS WITH 3D VECTOR ANTENNA

The in-lab validation of the 5G-based algorithms has been done based on the block diagram in Fig. 10. The in-lab set-up comprised one PC (Intel i7-8700, with CPU at 3.20 GHz, 32 GB RAM, and 1TB SSD) to host the LabVIEW to run the AoA and time delay estimation algorithm; one cabled PCI Express Switch Box x4 10 Port (CPS-8910) to connect the three USRPs to the PC's PCIe adapter; one PCIe adapter used in motherboard-level connections as an expansion card interface; several SMA cables for 10 MHz clock and PPS distribution for synchronization and another group for RF signal connection; a four-Way DC Pass Power Splitter (ZN4PD-272-S+) in the frequency range 500 - 2700 MHz at 50Ω to deliver multiple output signals with specific output phase and amplitude characteristics; three RIO USRPs (two NI USRP-2954R for receiving signals and one NI USRP-2953R for transmitting signal; a 3D vector antenna connection with 8 ports, among which 4 electric ports were used connect to the two receiver USRPs; one OctoClock CDA-2990 with 10MHz reference clock and PPS output to build multi-channel systems that are synchronized to a common timing source; and a GPS antenna to drive the external clock of the OctoClock. Mesaurements were performed at 2.1 GHz carrier frequency.

Several transmitter antennas have been used (e.g., monopole, Yagi); an example of the in-lab set-up with a Yagi antenna with 5dBi antenna gain and a frequency range between 700MHz and 6GHz is shown in Fig. 11. Data was collected under both LOS and NLOS scenarios. The obstacle used for NLOS measurements is also illustrated in the lower plot of Fig. 11.

Figure 11. lEFT plot: Lab picture with the Yagi antenna at the TX and the 3D VA at the RX. Left: LOS scenario; right plot: Obstacle used for NLOS scenario in the wave path.

The AoA algorithm has been implemented in LabVIEW 2021, as illustrated in Fig. 12.

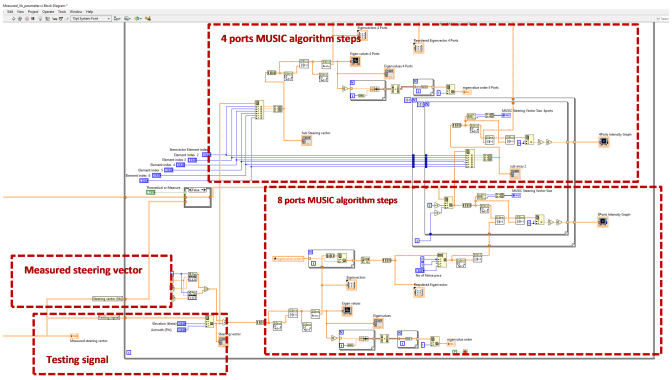

Figure 12. 3D-VA MUSIC Algorithm steps in LabVIEW.

Snapshot examples of AoA estimates under static and moving scenarios are depicted in Fig. 13 and Fig. 14, respectively and show perfect estimates under noiseless scenarios.

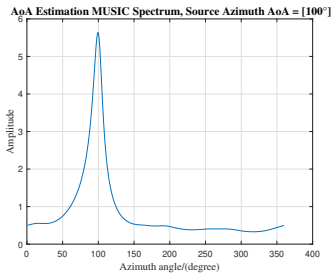

Figure 13. AoA estimation with 3D-VA at 100°.

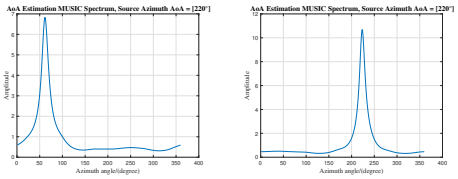

Figure 14. Snapshots of moving the Tx back and forth of different angles.

Part of our AoA measurements with this setup are now available in open source at [6]. The LOS detection algorithm testing via the in-lab set-up is still on-going; part of the measurements have already been collected and an example of correlation outputs under LOS and NLOS scenarios with SRS 5G signals is given in Fig. 15. Compared to the theoretical LOS/NLOS models of Fig. 9, the measured NLOS channel has a lower amount of multipath; the noise floor is higher in LOS compared with LOS case in both simulated and measured data.

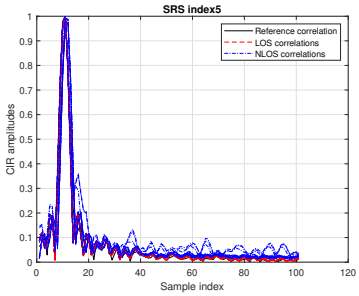

Figure 15. Examples of LOS and NLOS correlation outputs based on measured data with 5G SRS signals and 3D VA.

VII. Conclusion

In this paper, we demonstrate that positioning and sensing using angle and/or timing information combined with 5G reference signals and mmWave radar are promising complementary tools in future airport surveillance. The performances of 3D-VA have been evaluated in the context of AoA estimation. We have addressed the problem of LOS detection through ML algorithms. The testbed setup with the 3D-VA was described. Current 5G-based results show that a receiver can achieve promising accuracy (order of few meters positioning error and close to zero direction-estimation errors with suitable antennas) when receiver is in LOS connection with at least 3 base stations. We have also shown that NLOS scenarios can be detected wit accuracies as high as 90% with machine learning algorithms if enough training data is available. In order to further improve the positioning and direction-estimation results also in NLOS scenarios, the 5G-based surveillance solution, encompassing positioning, LOS detection, and radar-like sensing is to be further investigated through hybridization with additional sensors and possible map information. Measurements using the FMCW mmWave radar and obtained results prove the potential of using this type of radar for airport surveillance. We have assessed the mmWave radar performances in terms of range, angle and velocity calculation. We have also applied Machine Learning methods to classify targets and we have obtained an accuracy up to 90%. We encountered some constraints during the measurements such as the test environment not large enough (e.g. in external parking, the maximum depth is 130 meters), no control on the target presence and trajectory (e.g. for aircraft at Muret airfield which were sometimes out of reach of the radar) and limited collected data as outdoor measurements have been done during 3 days (1 day in external parking and 2 days at Muret airfield). This is different from measurement campaigns when the sensor is installed 24/7. Thus, we assume that positioning results could be ameliorated in more favourable testing environment, especially if the radar is adapted and trained for a specific airport. Future work will consist of a) completing the 5G-signal-based solution measurements with the 3D-VA and investigating MUSIC AoA estimates under various transmit powers and noise conditions, b) enhancing the ML applied to mmWave data, c) evaluating the system performance against equivalent A-SMGCS standards. This work will also feed the EUROCONTROL A-SMGCS Task force and the EUROCAE Working Group 41 on integrating new technical solutions into the A-SMGCS surveillance service and its performance framework.

Acknowledgment

This work was supported by SESAR Joint Undertaking (SJU) in project NewSense (grant 893917). The opinions expressed herein reflect the authors' view only. Under no circumstances shall the SJU be responsible for any use that may be made of the information contained herein. This work was also partly supported by the Academy of Finland, under the projects ULTRA (328226) and ACCESS (339519).

References

[1] G. Xiangyu, X. Guanbin, R. Sumit, and L. Hui, "Ramp-cnn: A novel neural network for enhanced automotive radar object recognition," *IEEE Sensors Journal*, vol. 21, no. 4, 2021.

[2] B. Dennis and A. Adrian, "mmwave radar sensors in robotics applications," *Texas Instruments*, 2017.

[3] G. Siddharth, K. R. Prabhat, K. Abhinav, Y. Phaneendra K., and R. C. Linga, "Target classification by mmwave fmcw radars using machine learning on range-angle images," *IEEE Sens. Journ.*, vol. 21(18), 2021.

[4] F. Mata, F. Grec, M. Azaola, F. Blázquez, A. Fernández, E. Dominguez, G. Cueto-Felgueroso, G. Seco-Granados, J. del Peral-Rosado, E. Staudinger, C. Gentner, M. Kasparek, C. Backert, D. Barlett, E. Serna, L. Ries, and R. Prieto-Cerdeira, ""preliminary field trials and simulations results on performance of hybrid positioning based on gnss and 5g signals," *Proceedings of the 33rd International Technical Meeting of the Satellite Division of The Institute of Navigation (ION GNSS+ 2020)*, September 2020, pp. 387-401.

[5] S. B. et al., ""positioning and sensing for vehicular safety applications in 5g and beyond," *IEEE Communications Magazine, vol. 59, no. 11, pp. 15-21*, November 2021.

[6] H. S. Obaid, B. Sun, C. Morlaas, B. Tan, and E.-S. Lohan, "Angle measurements with 3d vector antenna for localization purposes – open-access datasets," Jul 2022.

[7] T. Bo, L. Elena Simona, S. Bo, W. Wenbo, Y. Taylan, M. Christophe, M. P. Carlos David, A. Kanaan, B. S. Fathia, S. Alexandre, and E. Mohamed, "Improved sensing and positioning via 5g and mmwave radar for airport surveillance," in *SID 2021*, 2021.

[8] J. Duplouy, C. Morlaas, H. Aubert, P. Potier, P. Pouliguen, and C. Djoma, "Wideband and reconfigurable vector antenna using radiation pattern diversity for 3-d direction-of-arrival estimation," *IEEE Transactions on Antennas and Propagation*, vol. 67, no. 6, pp. 3586–3596, 2019.

[9] "Awr2243 evaluation module (awr2243boost) mmwave sensing solution, user's guide." Texas Instruments, February 2021.

[10] "Dca1000evm data capture card, user's guide." Texas Instruments, 2019.

[11] "Primary surveillance radar (psr); harmonised standard for access to radio spectrum; part 2: Air traffic control (atc) psr sensors operating in the frequency band 2 700 mhz to 3 100 mhz (s band)." ETSI EN 303 364-2, 2021-02.

[12] T. Mingxing and V. Quoc, "Efficientnetv2: Smaller models and faster training." https://arxiv.org/abs/2104.00298, 2021.

[13] X. Gao, G. Xing, S. Roy, , and H. Liu, "Ramp-cnn: A novel neural network for enhanced automotive radar object recognition," *IEEE Sensor Journal, 2020*, April 2022.

[14] A. Bochkovskiy, W. Chien-Yao, and M. L. Hong-Yuan, "Yolov4: Optimal speed and accuracy of object detection." https://arxiv.org/abs/2004.10934, April 2020.

[15] J. Zhang, J. Salmi, and E.-S. Lohan, "Analysis of kurtosis-based los/nlos identification using indoor mimo channel measurement," *IEEE Transactions on Vehicular Technology*, vol. 62, no. 6, pp. 2871–2874, 2013.

[16] J. Xie, W. Wang, and Z. Xu, "Identification of nlos condition in different scenarios based on wireless propagation features," in *2021 IEEE 4th International Conference on Electronic Information and Communication Technology (ICEICT)*, pp. 568–571, 2021.

[17] A. Morita, H. Iwai, and H. Sasaoka, "Identification of line of sight by cross polarization characteristic," in *2015 International Symposium on Antennas and Propagation (ISAP)*, pp. 1–4, 2015.

[18] N. Alsindi, Z. Chaloupka, and J. Aweya, "Entropy-based non-line of sight identification for wireless positioning systems," in *Ubiquitous Positioning Indoor Nav. and Location Based Service*, pp. 185–194, 2014.

[19] J. Li, Y. Chang, T. Zeng, and Y. Xiong, "Channel correlation based identification of los and nlos in 3d massive mimo systems," in *2019 IEEE Wireless Comm. and Network. Conf.*, pp. 1–6, 2019.

[20] K. Bregar and M. Mohorčič, "Improving indoor localization using convolutional neural networks on computationally restricted devices," *IEEE Access*, vol. 6, pp. 17429–17441, 2018.

[21] T. Suzuki and Y. Amano, "Nlos multipath classification of gnss signal correlation output using machine learning," *Sensors*, vol. 21, no. 7, 2021.

[22] J. Yoon, H. Kim, D. Seo, and H. Nam, "Performance comparison of nlos detection methods in uwb," in *2021 International Conference on Information and Communication Technology Convergence (ICTC)*, pp. 1486–1489, 2021.

[23] Y. Sun and L. Fu, "Stacking ensemble learning for non-line-of-sight detection of global navigation satellite system," *IEEE Transactions on Instrumentation and Measurement*, vol. 71, pp. 1–10, 2022.

[24] L. Flueratoru, E. S. Lohan, and D. Niculescu, "Self-learning detection and mitigation of non-line-of-sight measurements in ultra-wideband localization," in *2021 International Conference on Indoor Positioning and Indoor Navigation (IPIN)*, pp. 1–8, 2021.

[25] G. Barb and M. Otesteanu, "On the influence of delay spread in tdl and cdl channel models for downlink 5g mimo systems," in *2019 IEEE 10th Annual Ubiquitous Computing, Electronics & Mobile Communication Conference (UEMCON)*, pp. 0958–0962, 2019.